Available online at www.sciencedirect.com
ScienceDirect
Computers & Fluids 37 (2008) 12–23
computers & fluids
www.elsevier.com/locate/compfluid

Influence of combustion parameters on NO_x production in an industrial boiler

M.A. Habib [a,*], M. Elshafei [b], M. Dajani [b]

[a] Mechanical Engineering Department, King Fahd University of Petroleum and Minerals, Dhahran 31261, Saudi Arabia
[b] Systems Engineering Department, King Fahd University of Petroleum and Minerals, Dhahran 31261, Saudi Arabia

Received 11 June 2006; received in revised form 28 December 2006; accepted 14 April 2007
Available online 24 June 2007

Abstract

NO_x formation during the combustion process occurs mainly through the oxidation of nitrogen in the combustion air (thermal NO_x) and through oxidation of nitrogen with the fuel (prompt NO_x). The present study aims to investigate numerically the problem of NO_x pollution using a model furnace of an industrial boiler utilizing fuel gas. The importance of this problem is mainly due to its relation to the pollutants produced by large boiler furnaces used widely in thermal industrial plants. Governing conservation equations of mass, momentum and energy, and equations representing the transport of species concentrations, turbulence, combustion and radiation modeling in addition to NO modeling equations were solved together to present temperature and NO distribution inside the radiation and convection sections of the boiler. The boiler under investigation is a 160 MW, water-tube boiler, gas fired with natural gas and having two vertically aligned burners.

The simulation study provided the NO distribution in the combustion chamber and in the exhaust gas at various operating conditions of fuel to air ratio with varying either the fuel or air mass flow rate, inlet air temperature and combustion primary air swirl angle. In particular, the simulation provided more insight on the correlation between the maximum furnace temperature and furnace average temperatures and the thermal NO concentration. The results have shown that the furnace average temperature and NO concentration decrease as the excess air factor λ increases for a given air mass flow rate. When considering a fixed value of mass flow rate of fuel, the results show that increasing λ results in a maximum value of thermal NO concentration at the exit of the boiler at $\lambda = 1.2$. As the combustion air temperature increases, furnace temperature increases and the thermal NO concentration increases sharply. The results also show that NO concentration at exit of the boiler exhibits a minimum value at around swirl angle of 45°.

1. Introduction

NO_x formation during the combustion process in gas-fired boilers occurs mainly through the oxidation of nitrogen in the combustion air by two mechanisms known as thermal NO_x and prompt NO_x. The rate of thermal NO_x formation is directly affected by the combustion zone temperature and the oxygen concentration. Thermal NO can be reduced by decreasing the flame temperature or limiting the oxygen concentration. The formation of NO in industrial boilers is a very complicated problem due to many parameters that influence its formation process. These parameters include fuel to air ratio, inlet air temperature and combustion air swirl angle. The numerical calculation of the combustion process in industrial boilers is a three-dimensional problem that involves turbulence, combustion, radiation in addition to NO modeling. In the combustion chamber of a boiler, the heat transfer is dominated by radiation. Hence accurate prediction of the radiative heat transfer is necessary to obtain a correct estimate of the thermal boiler performance. In addition, correct computation of the thermal radiation is needed to accurately predict the temperature field as well as the heat fluxes at the walls of the boiler. Complex three-dimensional models

* Corresponding author.
E-mail address: mahabib@kfupm.edu.sa (M.A. Habib).

0045-7930/$ - see front matter © 2007 Elsevier Ltd. All rights reserved.
doi:10.1016/j.compfluid.2007.04.006

Nomenclature

A/F	air to fuel ratio
C_μ	empirical constant in the κ–ε turbulence model
f_μ	empirical constant in the κ–ε turbulence model
K	kinetic energy of turbulence
k_j	rate coefficients in Eqs. (9)–(12)
M	molecular weight
p	pressure
Pr_t	turbulent Prandtl number
T	temperature (K)
U_j	velocity components in the x_j directions
$\overline{U}_j$	average velocity components
u_j	fluctuating components of velocity
u	fluctuating component of velocity in the x-direction
x_j	space coordinate
Y	mass fraction of NO
x, y, z	coordinates

Greek symbols

δ	Kroneker delta
ε	rate of dissipation of the kinetic energy
λ	excess air factor, defined as the actual air-to-fuel ratio divided by the theoretical air-to-fuel value, $\lambda = (A/F)/(A/F)_{theoretical}$
μ	viscosity
ϕ	general field variable represented in the transport equation
ρ	density
σ_k	effective Prandtl number for κ
σ_ε	effective Prandtl number for ε
θ	swirl angle

Subscripts

avg	average value across the vertical plane passing through the burners
exh	average value across the boiler exit section
NO	nitrogen oxide
max	maximum value across the vertical plane passing through the burners

Superscript

—	time average

for equipment design and operational changes are usually based on computational fluid dynamics, CFD [19]. CFD models are founded on fundamental physical principles and can thus predict fluid flow and heat transfer properties within boilers and under specific operational conditions. Submodels such as combustion, turbulence, and NO_x formation can be added as subroutines [8]. The mechanisms of NO_x formation and correlations can be captured by mathematical models [19,8,12], and their dependence on furnace operating conditions and fuel composition.

Kokkinos et al. [17,18] applied some techniques for reducing NO_x emissions from tangentially fired boilers. They applied staged combustion along the combustors front and rear walls through rerouting the location of some fuel and oxidant feed ports. They used a numerical approach to optimize the design to minimize NO_x emissions and reported a decrease of 50% from baseline levels. A fully three-dimensional flow, heat transfer and combustion computer model was developed by Boyd et al. [3] for tangentially fired pulverized fuel furnaces. The complete model solves equations for gas momentum and mixing, particle trajectories and combustion and energy conservation with radiation transfer. They presented predictions of mixture fraction distributions for a model furnace. In their study of NO_x control for six tangentially fired boilers, Baubilis and Miller [2] indicated that experience with NO_x reduction modifications is still limited industry wide. Potential long term system impacts are not yet fully understood. Zheng et al. [35] presented numerical and experimental study on reduction of NO_x emissions in the furnace of a tangentially fired boiler under different operating conditions. A simplified NO_x formation mechanism model, along with the gas-particle multiphase flow model, was adopted. The prediction yielded encouraging results as compared to experimental data. The coal combustion behavior in a tangentially fired boiler furnace was numerically studied by Liu et al. [21] using a modified char combustion model.

Other recent studies [7,5,12] have involved the total flow and energy modeling of industrial gas furnaces. The focus in these studies was on improving the efficiency of furnaces and reducing NO_x pollution among other considerations. Measurements of the stability limits and temperature contour maps of flame inside a water-cooled tangentially fired model furnace were performed by Habib et al. [13]. The limits of ignition were found to depend on the inclination angle of the burners and on the temperature levels. A one-component model to represent oil- and gas-fired boilers was developed and implemented in a system simulation program by Handby and Li [15]. The objective of their study was to calculate the emissions of NO_x, CO and SO_x, in addition to prediction of the performance of the boiler. One-dimensional reaction rate equations were used to predict NO. It was found that NO_x formation could be calculated satisfactorily from established chemical rate equations in the case of gas-fired units, with separate consideration of the prompt and thermal routes. The results provided good prediction of heat transfer performance and reproduced the values and trends of emissions throughout the operating range of the boiler. An empirical relationship based on the adiabatic flame temperature and the air–fuel ratio was shown to work effectively over the

operating ranges encountered for both the gas and the oil firing unit. A comparison of the output of the model with tests carried out on commercial units showed that the model has the capability to represent both trends and absolute values, representing the thermal and emissions performance of such boilers.

A model of NO emissions for a power plant boiler was presented by Li and Thompson [19]. It is modeled from the extended Zeldovich mechanism and requires only a few physical parameters obtained from experiments. A set of new test data was used to compare the simulated values with real measurements. The research work was based on boiler unit with oil firing. Experiments were conducted to evaluate the different parameters for modeling NO. It was shown that good results were obtained from the model with real plant input variables. Responses of NO to changes in fuel flow rate, fuel air ratio and burner tilt were presented. The application of a full three-dimensional mathematical model to a fuel-oil-fired power station boiler was conducted by Coelho and Carvalho [6]. Several variants of thermal and fuel-NO formation models were applied to the prediction of NO concentration in a utility boiler. Models for thermal and fuel-NO formation were included and several variants of the models were employed. Predictions of temperature, O_2, CO_2, CO and NO mole fractions through inspection ports at the side wall were compared with measurements. It was shown that the predicted O_2, CO_2 and CO mole fractions are in good agreement with the available data. The temperature along the profile crossing the flame region was slightly under-estimated but it is in qualitative agreement with the measurements. The NO mole fraction, however, is significantly under-predicted. It was shown that the role of fuel-NO and the super-equilibrium of oxygen atom concentration are not responsible for the differences observed. The most probable reasons for the discrepancies were attributed to the errors in the temperature prediction and in the measurements.

Chong et al. [4] modeled the gaseous emissions emanating from the combustion of coal in a chain-grate stoker-fired boiler. The resultant models of the oxygen concentration, nitrogen oxides and carbon monoxide in the exhaust flue gas were able to represent the dynamics of the process and delivered accurate one-step-ahead predictions over a wide range of unseen data. CFD simulations were conducted by Mathur et al. [23] to investigate the effects of moisture in biomass/coal, particle injection locations, and flow parameters on carbon burnout and NO_x inside a 150 MW industrial boiler. The research objective of this study is to develop a three-dimensional combustor model for biomass co-firing and reburning applications using the Fluent CFD Code. Determination of NO_x emissions from strong swirling confined flames with an integrated CFD-based procedure was conducted by Frassoldati et al. [11]. The model used very detailed and comprehensive reaction schemes on the basis of the results obtained from CFD computations. The procedure was validated in the case of high swirled confined natural gas diffusion flames.

Based on the above literature search, it is clear that the problem of NO_x formation in industrial boilers although received much attention in regard of coal-fired boilers, a limited portion of research work was focused on gas-fired boilers. The present work is aimed at conducting a numerical investigation of the problem of the influence of the air to fuel ratio, the inlet combustion air temperature and the swirl angle on NO formation. CFD packages Fluent 6.1.22 were used for the calculations in the present work.

2. Description of the boiler model

The studied boiler considered in the present study is 160 MW, gas fired with natural gas, water-tube boiler, having two vertically aligned burners. The boiler is composed of a furnace (radiation section) and return tube bank (convection section). The boiler is used for production of superheated steam for process industry. The steam flow rate is 240 t/h. Steam pressure and steam temperature are 51 bar and 330 °C. The combustion chamber has 12.541 m length in the direction of flame, 4.579 m width of front wall and 7.925 m (distance between drums). A schematic of the boiler is shown in Fig. 1. The primary

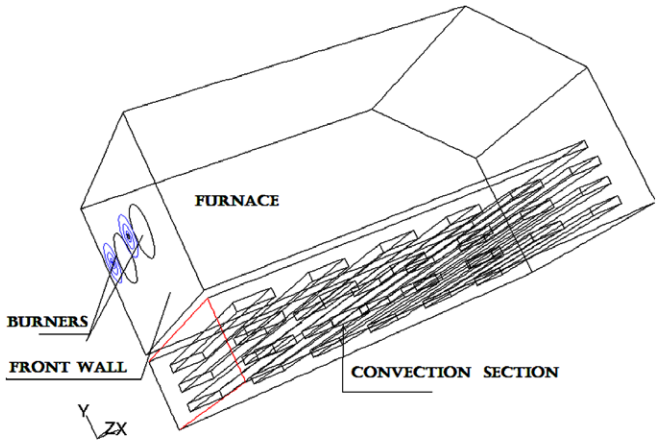

a. Furnace and convection section

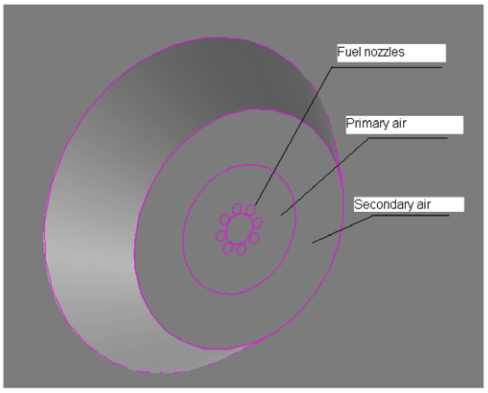

b. View of the burner.

Fig. 1. Configuration of the boiler.

air has a swirl angle of 45° and the secondary air has no swirl.

3. Mathematical formulation

The mathematical model is based on the numerical solution of the conservation equations for mass, momentum and energy, and transport equations for scalar variables. The equations, which are elliptic and three-dimensional were solved to provide predictions of the flow pattern, thermal and pollution characteristics of reacting flows inside a model of an industrial boiler. Operating parameters include the air to fuel ratio, combustion air temperature and swirl angle. The governing equations, turbulence model, the boundary conditions and the solution procedure are presented in the following sections.

3.1. The governing equations

The equations which govern the conservation of mass, momentum and energy as well as the equations for species transport may be expressed in the following general form [27,28]:

$$\frac{\partial}{\partial x_j}\left(\bar{\rho}\overline{U}_j\Phi + \bar{\rho}\overline{u_j\phi}\right) = \frac{\partial}{\partial x_j}\left[\Gamma_\Phi \frac{\partial \Phi}{\partial x_j}\right] + \bar{\rho}S_\Phi \tag{1}$$

where Φ is the dependent variable and u_j is the velocity component along the coordinate direction x_j. $\bar{\rho}$ is the fluid density; Γ_Φ is the diffusion coefficient and S_Φ is the source term.

Eq. (1) stands for the mass conservation equation when $\Phi = 1$; the momentum conservation equation when Φ is a velocity component; the energy equation when Φ is the stagnation enthalpy; or the transport equation of a scalar when Φ is a scalar variable such as mixture fraction. The present work utilized the κ–ε turbulence model [31]. The Reynolds stresses and turbulent scalar fluxes in the model are related to the gradients of the mean velocities and scalar variable, respectively, via exchange coefficients as follows [31]:

$$-\rho\overline{u_i u_j} = \mu_t\left(\frac{\partial \overline{U}_i}{\partial x_j} + \frac{\partial \overline{U}_j}{\partial x_i}\right) - \frac{2}{3}\rho k\delta_{ij} \tag{2}$$

$$-\rho\overline{u_j\phi} = \Gamma_\Phi \frac{\partial \Phi}{\partial x_j} \tag{3}$$

where μ_t is the turbulent viscosity and Γ_Φ is equal to μ_t/σ_Φ. The turbulent viscosity is modeled as

$$\mu_t = c_\mu \rho f_\mu K^2/\varepsilon \tag{4}$$

where c_μ and f_μ and σ_Φ are constants. The turbulent viscosity is thus obtained from the solution of the transport equations for κ and ε. RNG (renormalized group) turbulence model [32] was used to provide better results for vortex flows. The present work utilized the "eddy dissipation concept" (EDC) model to consider the turbulence–chemistry interaction [22]. In order to correctly predict the temperature distribution in the furnace a radiative transfer equation (RTE) for an absorbing, emitting and scattering medium was solved. Once the radiative intensity is obtained, the gradient of the radiative heat flux vector was found and substituted into the enthalpy equation to account for heat sources (or sinks) due to radiation. The solution of the RTE for this application was obtained using the discrete ordinates (DO) radiation model [26]. The blackbody spectral emissive power is calculated through using variables by Liu et al. [20] and Zhang et al. [34] based on expressions of Modak [24] and Smith et al. [30].

3.2. Boundary conditions

The velocity distribution is considered uniform at the inlet section with the velocity in the direction of the burner nozzle axis. Kinetic energy and its dissipation rate are assigned through a specified value of $\sqrt{K/\overline{U}^2}$ equal to 0.1 and a length scale, L, equal to the characteristic length of the inlet pipe/annulus. The boundary condition applied at the exit section is that of fully developed flow. At the wall boundaries, all velocity components are set to zero in accordance with the no-slip conditions. Kinetic energy of turbulence and its dissipation rate are determined from the equations of the turbulence model. The production of kinetic energy and its dissipation rate at the wall-adjacent cells are computed on the basis of the local equilibrium hypothesis. Under this assumption, the production of k and its dissipation rate are assumed to be equal in the wall-adjacent control volume. The ε equation is not solved at the wall-adjacent cells. Thus, the production of k at the node close to the wall is taken proportional to the square of the wall shear stress. The rate of dissipation, ε, at the node close to the wall is taken proportional to $k^{3/2}$ [31].

3.3. NO formation model

The combustion process considered in the present study has two opportunities for NO_x formation. The first is the thermal NO_x which is controlled by the nitrogen and oxygen molar concentrations and the temperature of combustion in excess of 1300 °C. The second is the prompt NO_x which is formed from molecular nitrogen in the air combining with fuel in fuel-rich conditions. This nitrogen then oxidizes along with the fuel and becomes NO_x during combustion. The mass transport equation for the NO species, including convection, diffusion, production and consumption of NO was solved. To consider the effect of residence time in NO mechanisms, a Lagrangian reference frame concept [9] is included through the convection terms in the governing equations written in the Eulerian reference frame. The principal reactions governing the formation of thermal NO_x are given as follows:

$$O + N_2 \underset{k-1}{\overset{k1}{\Longleftrightarrow}} N + NO \tag{5}$$

$$O_2 + N \underset{k-2}{\overset{k2}{\Longleftrightarrow}} O + NO \tag{6}$$

For thermal NO, the NO species transport equation is given by

$$\frac{\partial}{\partial x_j}(\rho U_j Y_{NO}) = \frac{\partial}{\partial x_j}\left[\Gamma_{NO}\frac{\partial Y_{NO}}{\partial x_j}\right] + S_{NO} \quad (7)$$

where Y_{NO} is the mass fraction of NO in the gas phase. The NO source term due to thermal NO_x mechanisms is given by

$$S_{NO,thermal} = M_{NO}\frac{d(NO)}{dt} \quad (8)$$

where M_{NO} is the molecular weight of NO, and $\frac{d(NO)}{dt}$ is computed from the following equation:

$$\frac{d(NO)}{dt} = \frac{2[O](k_1k_2[O_2][N_2] - k_{-1}k_{-2}[NO]^2)}{k_2[O_2] + k_{-1}[NO]} \quad (9)$$

The concentration [O] is given by the partial equilibrium [O] approach as

$$[O] = 36.64T^{0.5}[O_2]^{0.5}\exp(-27123/T) \quad (10)$$

where all the concentrations are having the units of mol/m^3.

The expressions for the rate coefficients (m^3/mol s) used in the NO model are given below [16]:

$$k_1 = 1.8\times10^8\exp(-38370/T) \quad (11)$$

$$k_{-1} = 3.8\times10^7\exp(-425/T) \quad (12)$$

$$k_2 = 1.8\times10^4 T\exp(-4680/T) \quad (13)$$

$$k_{-2} = 3.8\times10^3 T\exp(-20820/T) \quad (14)$$

The rate of formation of thermal NO is significant only at high temperatures (greater than 1800 K) because fixation of nitrogen requires the breaking of the strong N_2 triple bond. It is known that during combustion of hydrocarbon fuels, the NO formation rate can exceed that produced from direct oxidation of nitrogen molecules (i.e., thermal NO). Many investigations have shown that the prompt NO contribution to total NO from stationary combustors is small. This is investigated in the present work. The details of the formulation of prompt NO_x formation can be found in Foster et al. [10]. The turbulent mixing process results in temporal fluctuations in temperature and species concentration which will influence the characteristics of the flame in a nonlinear form. Thus, employing time-averaged composition and temperature in any model to predict the mean NO_x formation rate can result in significant errors. In the present work, temperature fluctuations were taken into account by considering the probability density functions which describe the time variation.

3.4. The solution procedure

The set of governing differential equations together with the boundary conditions are to be solved numerically by an iterative, line-by-line procedure [25]. The details of the calculation procedure can be found in previous work such as Habib and Whitelaw [14], Attya and Habib [1] and Shuja and Habib [29]. The investigators used CFD packages Fluent 6.1.22. IBM computer of one Giga RAM was used. A grid of 371,000 control volumes was considered. More grids were used in regions of large property gradients and in the vicinity of the walls. Thousand and five hundred iterations were required to reach convergence. A criterion for convergence was used such that the solution was considered to be converged when the maximum of the residuals of the continuity, U, V and W summed allover all the control volumes was less than 10^{-6}. The solution procedure first solves the partial differential equations for conservation of mass, momentum, energy and combustion species. Then, the transport equation for species NO is solved to provide the NO distributions. Grid independence tests for three different mesh sizes were carried out. The mesh sizes are 262000 (mesh 1), 371000 (mesh 2) and 474000 (mesh 3). The influence of the mesh refinement on the distribution of the temperature and the mole fraction of the NO formation along the axis of the lower burner are shown in Figs. 2a and 2b. The results indicate that increasing the grid size

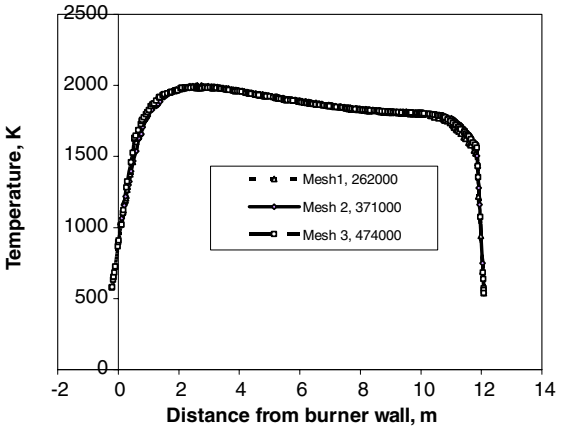

Fig. 2a. The influence of the mesh size on the distribution of the temperature along the axis of the lower burner.

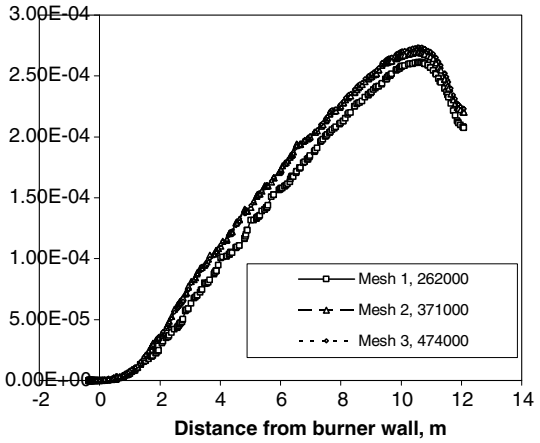

Fig. 2b. The influence of the mesh size on the distribution of the mole fraction of the NO formation along the axis of the lower burner.

from 262000 to 371000 has lead to around 1% difference in the temperature and 4% in the NO maximum values. Further increase to 474000 has lead to a negligible difference in temperature and of less than 0.6% in the NO concentration. Thus, the mesh of 371000 was considered suitable for the present calculations.

4. Results

4.1. Validation

In order to validate the computational procedure, comparison of the present calculations with the experimental data of Yaga et al. [33] was performed. The experimental data Yaga et al. [33] were obtained for the combustion process inside furnace of diameter of $D = 0.2$ m and 0.8 length. Methane gas at a flow rate of 0.2 Nm^3/h was burned with air at a rate of 1.9 Nm^3/h at stoichiometric equivalence ratio. The fuel was introduced through a circular pipe of 5 mm and the air annulus pipe has an outside diameter of 23 mm. Radial distributions of temperature and methane mole fractions were presented at a axial location of $x = 0.05D$. The comparisons of the calculated and measured data are shown in Figs. 3a and 3b. The calculated results of Yaga et al. [33] using large scale eddy simulation are also presented on the same figures. Figs. 2a and 2b indicate that the mole fraction of the methane fuel is well predicted by the numerical procedure. The centerline value is under-predicted by the present calculations. The radial temperature distributions, Figs. 3a and 3b indicate that the temperature is under-predicted at the centerline and good agreement is shown in other regions.

4.2. General flow features

The model is a three-dimensional boiler. The simulation study provided the NO_x distribution in the combustion chamber and in the exhaust gas at various operating conditions of fuel to air ratio of varying fuel mass flow rate or air mass flow rate, combustion air inlet temperature and combustion primary air swirl angle. In particular, the

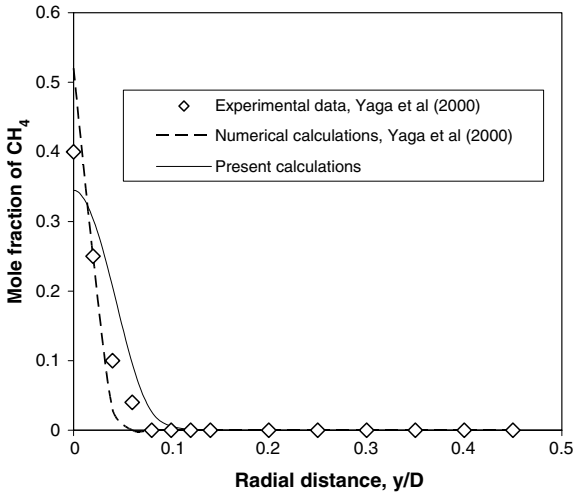

Fig. 3a. Comparison of calculated and measured distributions of mole fraction of CH_4 at $x/D = 0.05$.

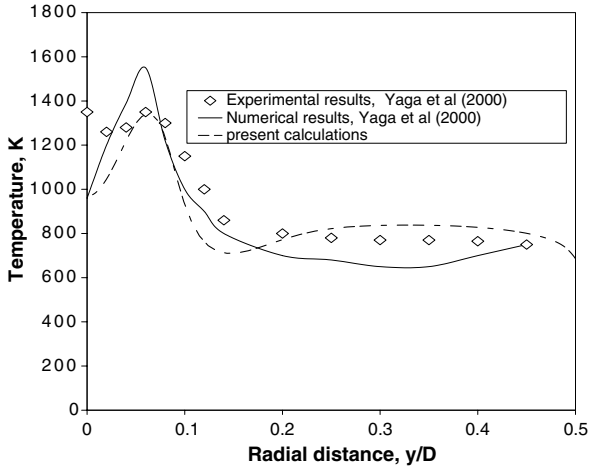

Fig. 3b. Comparison of calculated and measured temperature distributions at $x/D = 0.05$.

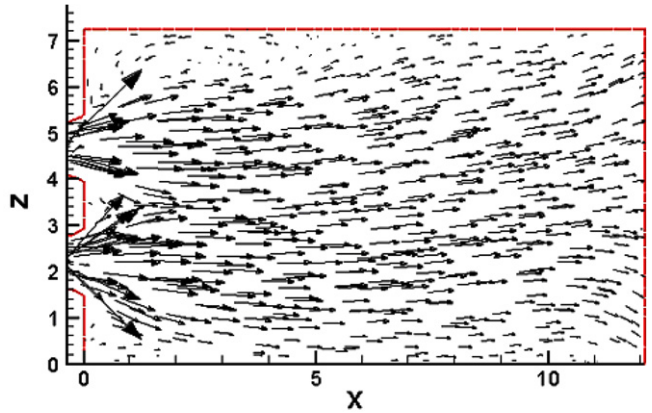

a. Vertical plane passing through the two burners, y=-2.24m

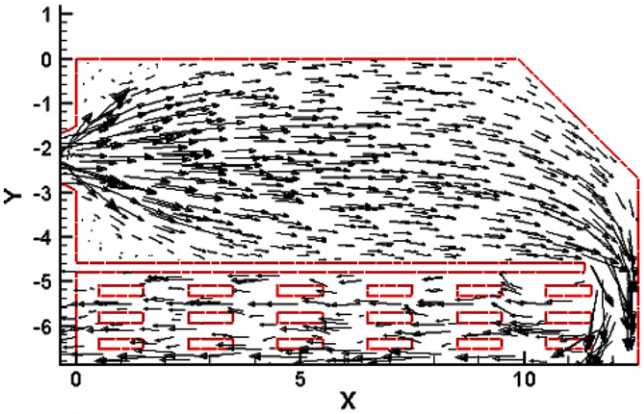

b. Horizontal plane passing through the upper burner, z=4.662m

Fig. 4. Velocity vectors of the flow field.

simulation provided more insight on the correlation between the maximum flame temperature, flame average temperatures and boiler exit temperature on the NO concentration. The general features of the flow and combustion characteristics are presented in Figs. 4–9 for the velocity vectors, temperature contours, NO and O_2 contours. These results are provided at the typical in-operation boiler as shown in Table 1. The results are presented at two different planes. The first is a vertical plane ($y = -2.24$ m) passing through the two burners and the second is a horizontal plane ($z = 4.662$ m) passing through the upper burner. The velocity vectors of the velocity magnitude at the typical case are shown in Fig. 4. The velocity of fuel at the burner edge (shown as long arrows) decreases as the fuel is mixed by turbulent diffusion with air due to air entrainment. The velocity along the burner axis decreases slightly towards the exit of the furnace. The flow velocity increases again in the passage to the convection section and maintains the same level throughout the convection chamber. The temperature distributions in a horizontal section passing through the two burners are shown in Fig. 5. The temperature distribution in a vertical section passing through the upper burner is shown in Fig. 6. The temperature reaches its maximum value of 2000 K at the flame front where stoichiometric mixture occurs. Temperature then decreases to around 1500 K at exit of the furnace before entering the convection section. The interaction of the two flames is shown in Fig. 6 where a complete mixing

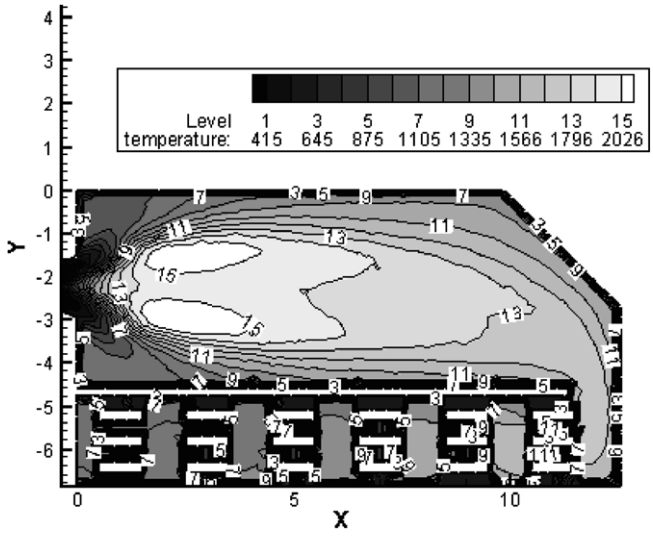

Fig. 5. Temperature (K) distributions at a horizontal plane passing through the upper burner, $z = 4.662$ m.

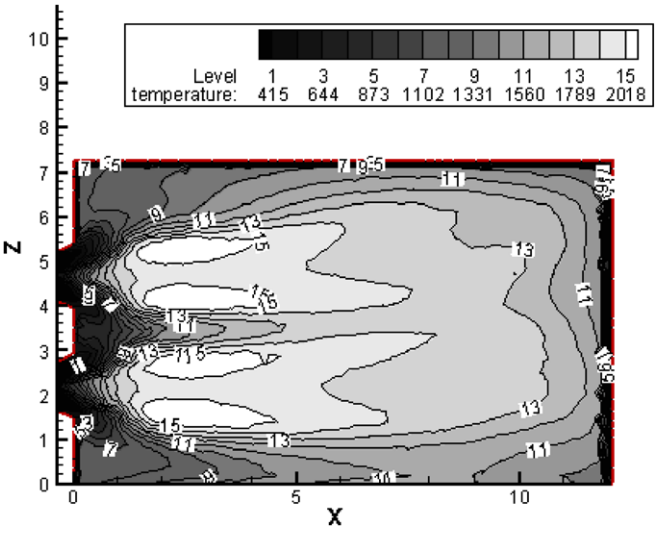

Fig. 6. Temperature (K) distributions at a vertical plane passing through the two burners, $y = -2.24$ m.

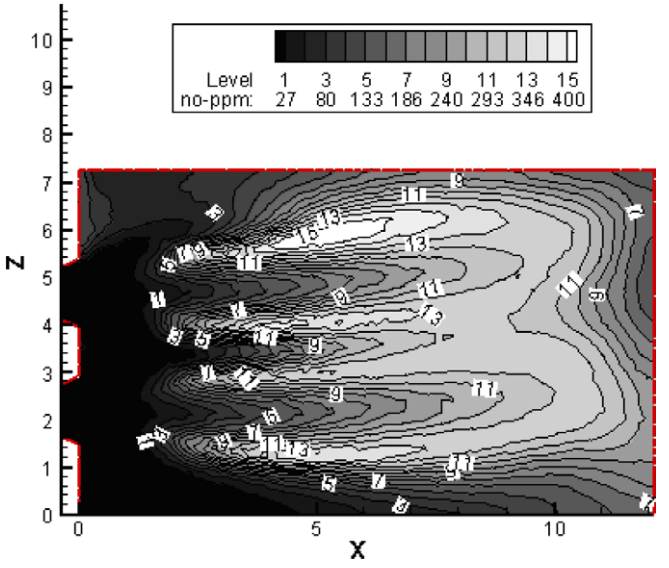

Fig. 7. Total NO (ppm) distributions at a vertical plane passing through the two burners, $y = -2.24$ m.

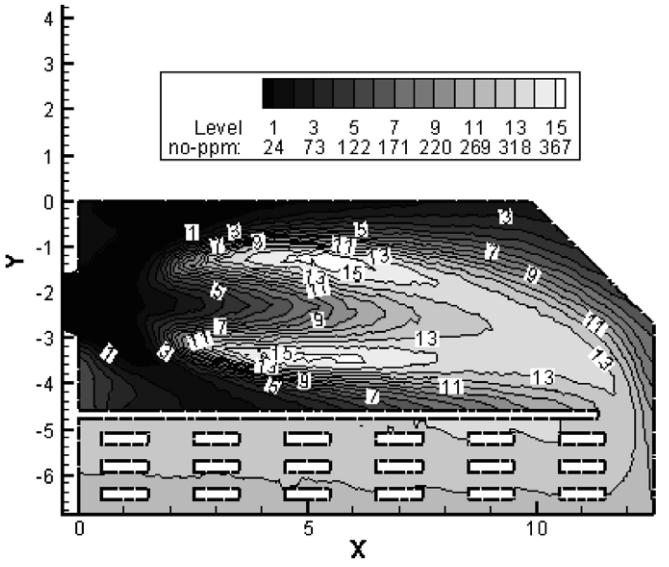

Fig. 8. Total NO (ppm) distributions at a horizontal plane passing through the upper burner, $z = 4.662$ m.

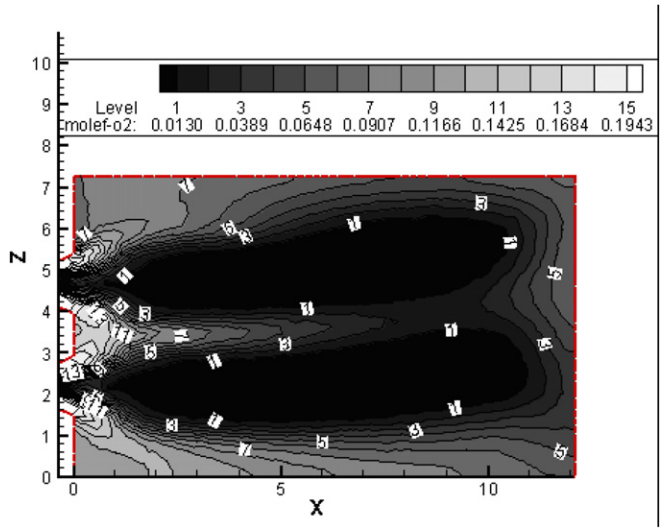

Fig. 9. O_2 (mole fractions) distributions at a vertical plane passing through the two burners, $y = -2.24$ m.

Table 1
Typical data for excess air factor $\lambda = 1.15$

Parameter	Value
Fuel flow rate	4.14 kg/s
Air flow rate	80.46 kg/s
Steam pressure	51 bar
Steam temperature	538 K
Fuel	Methane
Steam flow rate	240 t/h
Swirl angle, primary air	45°
Radial angle for fuel	45°
Air temperature	300 K

occurs, thus, providing quasi-homogeneous temperature in the last one-third of the furnace.

Fig. 7 presents the distribution of NO in the burners' plane. The NO value reaches its maximum value at the flame front. This is attributed to the elevated value of temperature at these locations which result in elevated value of the thermal NO. The NO value decreases towards the exit of the furnace. Fig. 8 shows the NO distribution in a horizontal plane and shows that NO stays unchanged in the convection part (tube bank passage). This is attributed to the low temperature values. The distributions of the mole fraction of oxygen in a horizontal section passing through the two burners are shown in Fig. 9. The oxygen concentration is reaching its minimum values at the locations of maximum temperature.

4.3. Temperature and NO results

Figs.10–17 present the influence of the different operating conditions of fuel to air ratio of varying fuel or air mass flow rates, inlet combustion air temperature and combustion air swirl angle on the maximum and average tempera-

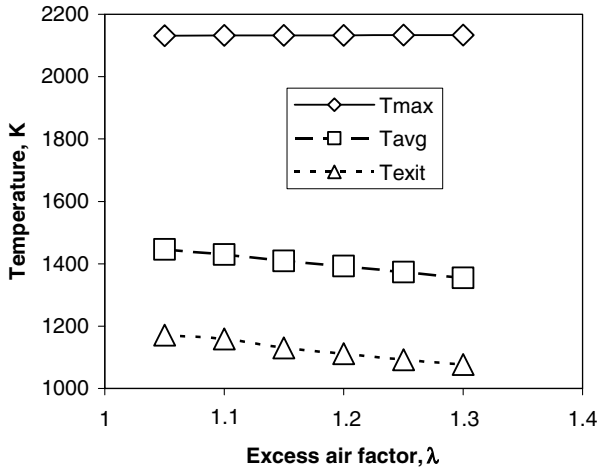

Fig. 10. Influence of A/F ratio (fixed air mass flow rate) on the temperature profiles. Conditions are as given in Table 1.

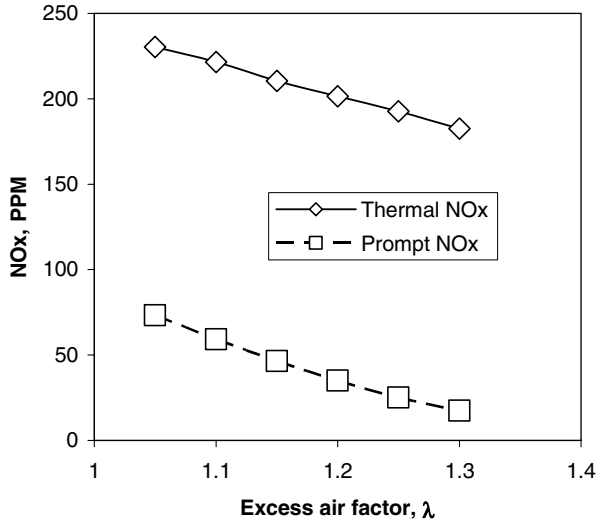

Fig. 11. Influence of A/F ratio (fixed air mass flow rate) on the NO profiles. Conditions are as given in Table 1.

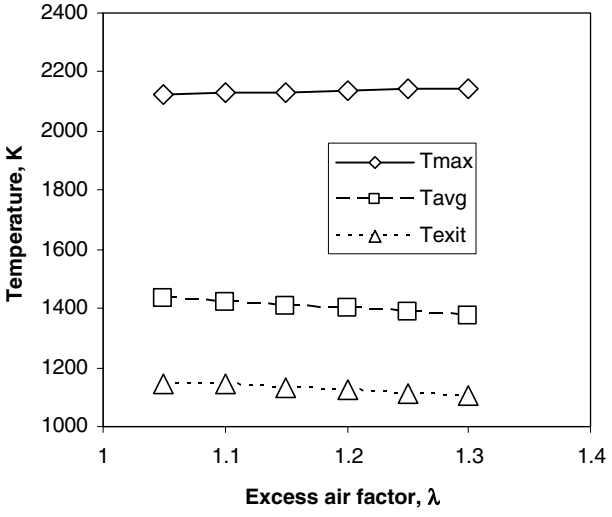

Fig. 12. Influence of A/F ratio (fixed fuel mass flow rate) on the temperature profiles. Conditions are as given in Table 1.

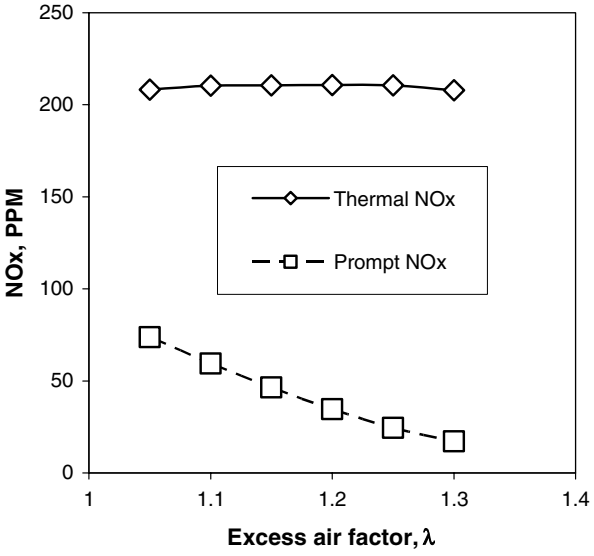

Fig. 13. Influence of A/F ratio (fixed fuel mass flow rate) on the NO profiles. Conditions are as given in Table 1.

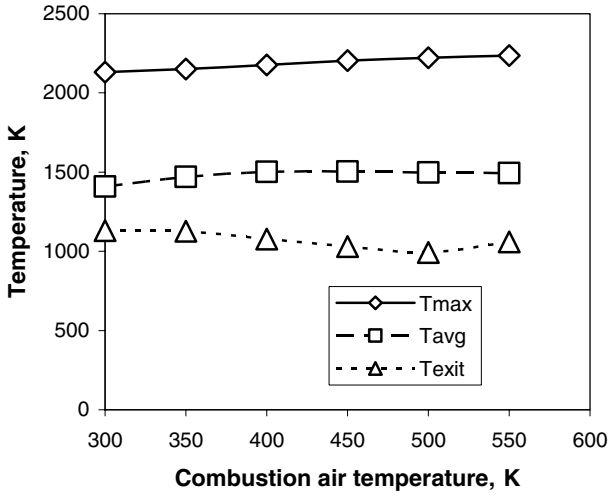

Fig. 14. Influence of combustion air temperature on the temperature profiles. Conditions are as given in Table 1.

ture inside the furnace as well as the temperature and NO concentration at the exit of the boiler. The mass-averaged value was used to present the average temperature. Those influences are given in the following (Table 2).

4.3.1. Influence of air to fuel ratio

Two cases are considered; the first case considers change of air to fuel ratio at a fixed fuel mass flow rate. The second case considers change of air to fuel ratio at a fixed fuel mass flow rate. In both cases, the mixture was kept at lean conditions at all the considered values of fuel to air ratio. Fig. 10 shows the influence of the air to fuel ratio at a fixed air mass flow rate on the temperature distributions. The air to fuel ratio is expressed in terms of the excess air factor, λ. The excess air factor is defined as the air to fuel ratio

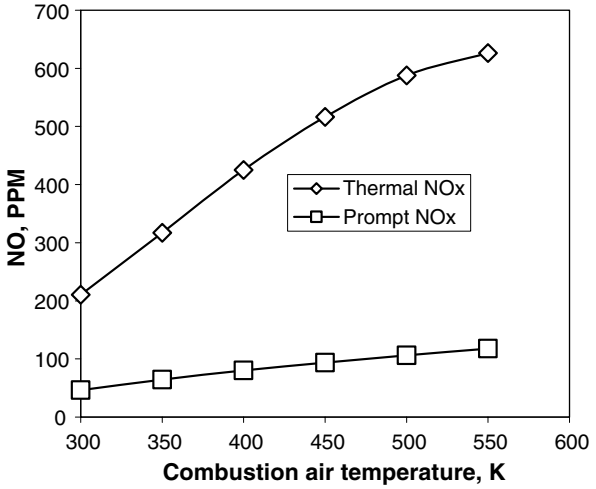

Fig. 15. Influence of combustion air temperature on the NO profiles. Conditions are as given in Table 1.

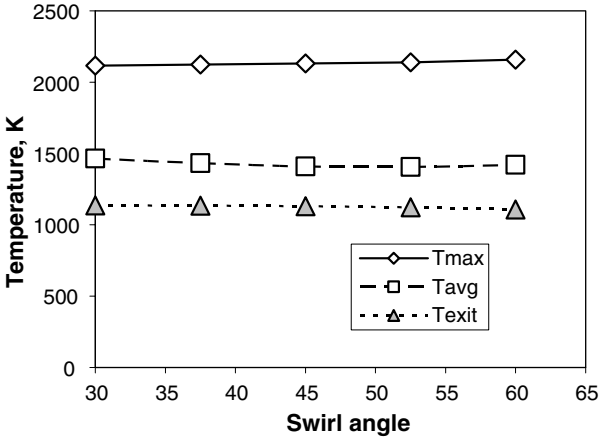

Fig. 16. Influence of swirl angle on the temperature profiles. Conditions are as given in Table 1.

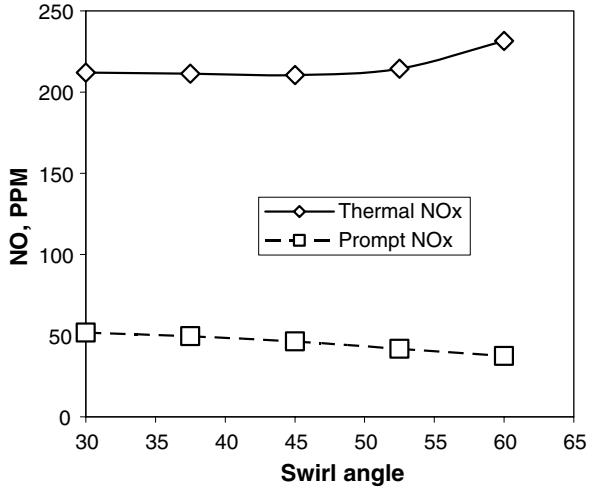

Fig. 17. Influence of swirl angle on the NO profiles. Conditions are as given in Table 1.

Table 2
Temperature and NO results

Parameter (changed)	Parameter value	Furnace maximum temperature	Furnace average temperature	Furnace exhaust temperature	NO concentration	
					Thermal	Prompt
$T = 300$						
Fuel flow	$\lambda = 1.05$	2131.6	1446.1	1171.5	230.3	73.2
Fuel flow	$\lambda = 1.1$	2132.5	1429.2	1158.6	221.5	59.2
Fuel flow	$\lambda = 1.15$	2132	1409	1130	210.5	46.4
Fuel flow	$\lambda = 1.2$	2132.8	1392.2	1111.9	201.5	35
Fuel flow	$\lambda = 1.25$	2133.8	1372.9	1092.1	192.6	25.4
Fuel flow	$\lambda = 1.3$	2133	1354.4	1076.5	182.6	17.5
Air flow	$\lambda = 1.05$	2122.3	1430.9	1142.6	208.3	73.8
Air flow	$\lambda = 1.1$	2128	1420	1144	210.4	59.4
Air flow	$\lambda = 1.15$	2132	1409	1130	210.5	46.4
Air flow	$\lambda = 1.2$	2136.6	1397.8	1122.9	210.7	34.7
Air flow	$\lambda = 1.25$	2141.2	1385.2	1114.6	210.6	24.4
Air flow	$\lambda = 1.3$	2144.7	1372	1108.4	207.9	17.1
Air temperature	$T = 300$	2132	1409	1130	210.5	46.4
Air temperature	$T = 350$	2151.3	1469.7	1126.8	316.9	64.3
Air temperature	$T = 400$	2176.2	1502.3	1077.9	425.1	80.1
Air temperature	$T = 450$	2204.8	1503.9	1029.1	516.6	93.7
Air temperature	$T = 500$	2221.9	1497.6	991.7	588	106.1
Air temperature	$T = 550$	2235	1494.1	1059.2	626.3	117.9
Swirl angle	30	2116.8	1465.8	1137.1	212.1	51.9
Swirl angle	37.5	2123.2	1431.8	1134.6	211.3	49.7
Swirl angle	45	2132	1409	1130	210.5	46.4
Swirl angle	52.5	2139.7	1405.4	1123.9	214.4	41.9
Swirl angle	60	2158.8	1420	1107.7	231.6	37.5

divided by the theoretical value. It is shown that although the furnace maximum temperature is almost fixed, the average furnace temperature as well as the boiler exit temperature decrease as the A/F ratio increases. As the air flow rate is increased above the theoretical value, the boiler input energy per kg of flue gases is reduced and, thus, the exhaust gas temperature decreases. The results of Fig. 11 show that the NO concentration decreases as the air to fuel ratio λ increases for a given air mass flow rate. The NO concentration is proportional to the temperature which exhibits continuous decrease with A/F as shown in Fig. 10. Fig. 12 shows the influence of A/F ratio at fixed fuel mass flows rate on the temperature profiles. Similar to Fig. 10, the furnace average temperature and the exhaust gas temperature decrease with A/F ratio. However, in this case, the furnace maximum temperature increases. When considering a fixed value of fuel mass flow rate, the results, Fig. 13, show that increasing λ results in increased thermal NO concentration at the exit of the boiler achieving amaximum value at $\lambda = 1.2$. Figs. 10–13 show that the prompt NO decreases monotonically with the air to fuel ratio.

4.3.2. Influence of combustion air temperature

The influence of combustion air temperature is shown in Fig. 14. As the inlet combustion air temperature increases, the furnace maximum temperature increases. The furnace average temperature increases up to $T = 450$ K but shows a decrease at higher combustion air temperatures. The exhaust temperature shows a minimum value at combustion air temperature of 500 K. As the exhaust temperature decreases, the dry gas loss is reduced and the thermal efficiency is improved. On the contrary to this, thermal NO and prompt NO, Fig. 15, increase with increased exhaust gas temperature. It is known that NO increases with temperature. As the combustion air temperature increases, and furnace temperature increases and NO concentration increases. It also appears that thermal NO formation is highly dependent on temperature. In fact, the thermal NO_x production rate doubles for every 90 K temperature increase beyond 2100 K.

4.3.3. Influence of swirl angle

Fig. 16 shows the influence of swirl angle θ. The figure indicates an increase in the maximum furnace temperature and a reduction in exhaust gas temperature as swirl angle is increased. The average temperature decreases until a value of swirl angle of 52.5° is reached and then increases. As θ increases, thermal NO, Fig. 17, decreases showing a minimum at $\theta = 45°$. Higher swirl angle leads to faster mixing of the fuel and air, thus, lowering the temperature levels of the flame and reducing the NO emissions. The results also show that further increase in the swirl number results in increased furnace maximum temperature and increased values of thermal NO concentrations at exit of the boiler. This may be attributed to the very high maximum temperature values.

5. Conclusions

The simulation provided insight on the correlation between the maximum furnace temperature, furnace average temperatures and average exhaust gas temperature on the NO concentration. The results have shown that the increase in excess air factor λ at a given air mass flow rate results in a reduced exit temperature and reduced NO concentrations. When considering a fixed value of mass flow rate of fuel, the results show that increasing λ results in maximum value of thermal NO concentration at the exit of the boiler at $\lambda = 1.2$. As the combustion air temperature increases, furnace temperature increases and thermal NO concentration increases sharply. The results also show that NO concentration at exit of the boiler exhibits a minimum value at around swirl angle of 45°. The results of this simulation could help in improving the predictive emission monitoring techniques, more effective instrumentation and monitoring of the combustion conditions and better control of the boiler.

Acknowledgment

The authors acknowledge the support of King Fahd University of Petroleum and Minerals during all the phases of this project.

References

[1] Attya AM, Habib MA. The influence of spray characteristics and air preheat on the flame properties in a gas turbine combustor. In: Nejat T, editor. Multi-phase transport and particulate phenomena; 1990.
[2] Baubilis DC, Miller JA. Utility perspective: NO_x control for six tangentially-fired boilers, fossil plant retrofit & repowering and fossil plant performance improvement. Fifth international conference and exhibition for the power generation industries – Power-Gen, vols. 11–12. Houston, TX, USA: Power-Gen; 1992. p. 297–308.
[3] Boyd RK, Roscarel KJ, Kent JH. Gas flow and mixing in a tangentially fired furnace. In: Third Australasian conference on heat and mass transfer, St. Leonards, May 13–15; 1985. p. 51–8.
[4] Chong AZS, Wilcox SJ, Ward J. Prediction of gaseous emissions from a chain grate stoker boiler using neural networks of ARX structure. IEE Proc Sci Meas Technol 2001;148(3):95–102.
[5] Chungen Y, Caillat S, Harion J-L, Baudoin JB, Perez E. Investigation of the flow, combustion, heat transfer and emissions from a 609 MW utility tangentially fired, pulverized coal boiler. Fuel 2002;81:997–1006.
[6] Coelho PJ, Carvalho MG. Mathematical modeling of NO formation in a power station boiler. Combust Sci Technol 1995;108:363–82.
[7] Coelho PJ, Carvalho MG. Evaluation of a three-dimensional mathematical model of a power station boiler. J Gas Turb Power 1996;118:887–95.
[8] Dong W. Design of advanced industrial furnaces using numerical modeling method, Ph.D. Thesis. Department of Materials Science and Engineering, Stockholm: KTH; 2000. ISBN 91-7170-500-7.
[9] Fluent 6.1 user's guide, Fluent Inc., Centerra Research Park, 10 Cavendish Court, Lebanon, NH 03766, USA; 2003.
[10] Foster T, Dupont V, Poukashanian M, Williams A. Low-NO_x water-heating appliances. J Inst 1994;67:101–8.
[11] Frassoldati A, Firgerio S, Colombo E, Inzoli F, Faravelli T. Determination of NO_x emissions from strong swirling confined flames with an integrated CFD-based procedure. Chem Eng Sci 2005;11:2851–69.
[12] Habib MA, Ben-Mansour R, Antar MA. Flow field and thermal characteristics in a model of a tangentially fired furnace under different conditions of burner tripping. J Heat Mass Transfer 2004;2. doi:10.1007/s00231-004-0593-6.
[13] Habib MA, El-Mahallawy FM, Abdel-Hafez A, Nasseef N. Stability limits and temperature measurements in a tangentially-fired model furnace. Energy, Int J 1992;17(3):283–94.
[14] Habib MA, Whitelaw JH. The calculation of turbulent flow in wide angle diffusers. Numer Heat Transfer 1982;5:145–64.
[15] Handby VI, Li G. Modeling of thermal emissions performance of commercial boilers. Int J Heat Ventil Air-Condition Refrig Res 1997;3(2):101–11.
[16] Hanson RK, Salimian S. Survey of rate constants in H/N/O systems. In: Gardiner WC, editor. Combustion chemistry; 1984. p. 361.
[17] Kokkinos A, Wasyluk D, Adams D, Yavorsky R, Brower M. B&W's experience reducing NO_x emissions in tangentially-fired boilers. The US EPA/DOE/EPRI combined power plant air pollutant control symposium; the mega symposium, August 20–23, Chicago, Illinois, USA; 2001.
[18] Kokkinos A, Wasyluk D, Brower M, Berna JJ. Reducing NO_x emissions in tangentially-fired boilers – a new appraoch, In: ASME international joint power generation conference, July 24–25, Miami, FL, USA; 2000.
[19] Li N, Thompson S. A simplified non-linear model of NO_x emissions in a power station boiler. In: UKACC international conference on control '96, 2–5 September, no. 427; 1996. p. 1016–21.
[20] Liu F, Becker HA, Bindar Y. A comparative study of radiative heat transfer modeling in gas-fired furnaces using the simple grey and the weighted-sum-of-grey-gases models. Int J Heat Mass Transfer 1998;41:3357–71.
[21] Liu XJ, Xu XC, Fan HL. Further studies on the coal combustion behavior in the tangentially fired boiler furnace. In: Proceedings of the Chinese society of electrical engineering, vol. 21, no. 1; 2001. p. 80–4.
[22] Magnussen BF, Hjertager BH. On mathematical models of turbulent combustion with special emphasis on soot formation and combustion. In: 16th Symposium (Int'l.) on combustion. The Combustion Institute; 1976.
[23] Mathur MP, Gera D, Freeman M. Computational fluid dynamics modeling analysis of combustors. In: 2001 Joint AFRC/JFRC/IEA. Combustion symposium, Kauai, HI, September 9–12; 2001.
[24] Modak AT. Radiation from products of combustion. Fire Res 1979;1:339–3361.
[25] Patankar SV. Numerical heat transfer and fluid flow. 1st ed. Taylor and Francis; 1980.
[26] Raithby GD, Chui EH. A finite-volume method for predicting a radiant heat transfer in enclosures with participating media. J Heat Transfer 1990;112:415–23.
[27] Reynolds WC. Fundamentals of turbulence for turbulence modeling and simulation, Lecture notes for Von Karman Institute, Agard Report No. 755; 1987.
[28] Shih TH, Liou WW, Shabbir A, Zhu J. A new k–ε eddy-viscosity model for high Reynolds number turbulent flows – model development and validation. Comput Fluids 1995;24(3):227–38.
[29] Shuja SZ, Habib MA. Fluid flow and heat transfer characteristics in axisymmetric annular diffusers. Comput Fluids 1996;25(2):133–50.
[30] Smith TF, Shen ZF, Friedman JN. Evaluation of coefficients for the weighted sum of gray gases model. J Heat Transfer 1982;104:602–8.
[31] Versteeg HK, Malalasekera W. An introduction to computational fluid dynamics; the finite volume method. Longman Scientific and Technical; 1995.
[32] Wilcox DC. Turbulence modeling for CFD. DCW Industries; 2000.

[33] Yaga M, Sasada K, Yamamoto T, Aoki H, Miura T. An eddy characteristic time modeling in LES for gas turbine combustor Mitsuru. In: Proceedings of 2000 international joint power generation conference, Miami Beach, FL, July 23–26; 2000. p. 1–6.

[34] Zhang L, Soufiani A, Taine J. Spectral correlated and non-correlated radiative transfer in a finite axisymmetric system containing an absorbing and emitting real gas-particle mixture. Int J Heat Mass Transfer 1988;31(11):2261–72.

[35] Zheng Y, Fan J, Ma Y, Sun P, Cen K. Computational modeling of tangentially fired boiler II NO_x emissions. Chin J Chem Eng 2000;8(3):247–50.